IEEE Access
Multidisciplinary | Rapid Review | Open Access Journal

Received January 20, 2018, accepted March 27, 2018, date of publication April 6, 2018, date of current version April 25, 2018.

Digital Object Identifier 10.1109/ACCESS.2018.2823982

A Solution of Optimal Power Flow Incorporating Wind Generation and Power Grid Uncertainties

JINQING LUO, LIBAO SHI, (Senior Member, IEEE), AND YIXIN NI, (Senior Member, IEEE)
National Key Laboratory of Power Systems in Shenzhen, Graduate School at Shenzhen, Tsinghua University, Shenzhen 518055, China

Corresponding author: Libao Shi (shilb@sz.tsinghua.edu.cn)

This work was supported by the National Natural Science Foundation of China under Grant 51777103.

ABSTRACT This paper proposes a novel approach for the solution of optimal power flow with consideration of uncertainties caused by wind generation and various factors in the power grid. Regarding the uncertainties studied here, multiple types of uncertainty modeling techniques are applied during research. Evidence theory and extended affine arithmetic are employed and mixed as the framework of uncertainty propagation to fuse probability distributions, possibility distributions, and intervals so as to obtain the best possible probability bounds, and the dependence among variables is handled by copula theory and affine arithmetic. Moreover, the uncertainty of wind farm active power and the characteristic of wind farm reactive power are modeled and integrated into the power flow calculation. An enhanced particle swarm optimization algorithm with introduction of fitness comparison and constraint handling techniques under the evidence theory framework is applied to the solution of this problem. The proposed model and method are tested on the IEEE 30-bus standard test system and a real-sized 183-bus power system to demonstrate the validity and effectiveness.

INDEX TERMS Affine arithmetic, evidence theory, optimal power flow, particle swarm optimization.

I. INTRODUCTION

The development of renewable energy has received a great boost in recent years due to depletion of fossil fuels and environmental concerns. Wind power, being abundant, widely distributed, clean and increasingly cost-effective, rises among the fastest growing renewable energy resources. But it is intermittent and fluctuant in nature and brings uncertainties to power systems. Besides, other elements in power systems like loads are also variable and would not be accurately represented by deterministic values. As wind power penetration reaches to a high level, the corresponding uncertain factors should be elaborately considered for power system planning and operation.

Optimal power flow (OPF) is considered as one of the most important tools to study and improve power system security and reliability. The most common branch of OPF incorporating uncertainties is the probabilistic OPF. Numerical approaches like Monte Carlo simulation (MCS) [1] have been adopted to solve OPF problem and further improved by some techniques like quasi-random sequence and ninth-order polynomial normal transformation [2]. The sampling-based algorithm can provide highly accurate results, but at the cost of heavy computational burden due to the repeated deterministic OPF calculations, making it unattractive for large-scale power systems. In comparison, analytical approaches to the probabilistic OPF are computationally more efficient via linearization of power flow equations. In this aspect, some notable examples including the first-order second-moment method [3], the cumulant method [4], and the Gaussian mixture model method [5] etc., have been tried with varying degrees of success. However, the accuracy of solution obtained by an analytical approach depends on whether the uncertainty propagation can be well represented by linear functions. Given that a probability distribution is easier to be approximated than a nonlinear transformation, some approximate approaches like the point estimation method [6] and the unscented transformation method [7] have been developed to obtain the properties of probability distributions of output variables.

The possibility theory can be used to describe the uncertain quantities when the available information is insufficient to construct appropriate probability distributions, and it has been successfully applied to study OPF problem. In this paradigm, input variables, objective function values, and

constraint violations are all represented by fuzzy converted to crisp linear programming [8], [9] or applying metaheuristic optimization algorithms with fuzzy techniques [10].

If only the ranges of uncertain variables are known, the interval-based methods can be utilized for OPF to calculate the lower and upper bounds of variables. The boundary OPF solution can be obtained by primal-dual interior point method [11]. Another approach is to employ the self-validated affine arithmetic (AA) and treat the uncertain variables in OPF problem as affine forms [12]. A generic mathematical programming problem and a knowledge-based noise symbol reduction technique under this framework have been proposed in [13].

The aforementioned research methods have been applied to study the uncertain OPF problem with different intentions. However, the available statistics associated with a power system might not be consistent enough for all uncertain factors to be accurately represented by only one type of mathematical model. In this case, applying probabilistic, possibilistic, or interval methods to the solution of OPF could lead to an inaccurate or even incorrect result. This paper aims to propose a hybrid approach, allowing each uncertain variable to be described by the most suitable model and fusing their probability distributions, possibility distributions, and intervals to obtain the best possible probability bounds for the OPF problem integrated with wind generation and power grid uncertainties. In this work, the evidence theory (ET), being compatible with probability theory, possibility theory, and interval analysis, and AA, extended to quadratic terms for second-order correlations, are combined for the uncertainty propagation. An enhanced particle swarm optimization (EPSO) incorporating uncertainty handling techniques under ET is applied to the solution of the uncertain OPF. The validity of the proposed model and method is verified on the IEEE 30-bus standard test system and a real-sized 183-bus power system.

The remaining of the paper is organized as follows. Section II introduces the deterministic model and solution of power flow with wind generation integration. In Section III, the modeling of uncertain OPF with wind generation and power grid uncertainties under the mixed ET and AA framework is addressed. An EPSO method is applied for the solution of the uncertain OPF problem, and the details can be found in Section IV. Case studies are carried out to demonstrate the validity of the proposed model and method in Section V, and finally, Section VI draws the concluding remarks.

II. DETERMINISTIC POWER FLOW WITH WIND GNERATION

A. WIND FARM ACTIVE POWER WITH CONSIDERATION OF THE WAKE EFFECT

A wind farm consists of tens or even hundreds of wind turbine units. Due to the wake effect, a turbine located downwind of another turbine captures a reduced wind speed and produces less active power. This paper adopts a single active power P_{wf} versus wind speed v curve [14], instead of summing up all wind turbine power outputs, to calculate the wind farm active power with consideration of the wake effect:

$$P_{\mathrm{wf}} = \begin{cases} 0 & v < v_{\mathrm{ci}}/\xi_{\mathrm{wf}},\ v \geq v_{\mathrm{co}} \\ \dfrac{(\xi_{\mathrm{wf}} v)^3 - v_{\mathrm{ci}}^3}{v_{\mathrm{r}}^3 - v_{\mathrm{ci}}^3} P_{\mathrm{wfr}} & v_{\mathrm{ci}}/\xi_{\mathrm{wf}} \leq v < v_{\mathrm{r}}/\xi_{\mathrm{wf}} \\ P_{\mathrm{wfr}} & v_{\mathrm{r}}/\xi_{\mathrm{wf}} \leq v < v_{\mathrm{co}} \end{cases} \quad (1)$$

where P_{wfr} is the installed capacity of wind farm; v_{ci}, v_{r}, and v_{co} are the cut-in, rated, and cut-out wind speeds respectively; ξ_{wf} is the wake effect attenuation coefficient of wind farm and can be obtained by aggregating the attenuation coefficients of all wind turbines:

$$\xi_{\mathrm{wf}} = \sqrt[3]{\frac{1}{n_{\mathrm{wt}}} \sum_{i=1}^{n_{\mathrm{wt}}} \xi_i^3} \quad (2)$$

where ξ_i is the wake effect attenuation coefficient of wind turbine i, calculated from the specific wake effect model of wind farm; n_{wt} is the number of wind turbines.

B. CHARATERISTIC OF WIND FARM REACTIVE POWER

Each type of wind turbine has its unique reactive power characteristic, which should be reflected in power flow calculation. In this paper, the doubly-fed induction generator (DFIG) and the permanent magnet synchronous generator (PMSG) are examined to take into account the reactive power exchange between the wind farm and the power system. Here, a wind farm is represented by an equivalent wind turbine model for simplicity.

For a DFIG-based wind farm, the simplified equivalent circuit model proposed in [15] is applied, of which the stator side power factor is maintained constant by controlling the magnitude and phase angle of the voltage supplied to the rotor winding. Neglecting the rotor side reactive power, the wind farm reactive power Q_{wf} can be calculated via the following quadratic equation:

$$a_Q \left(\frac{Q_{\mathrm{wf}}}{n_{\mathrm{wt}}}\right)^2 + b_Q \frac{Q_{\mathrm{wf}}}{n_{\mathrm{wt}}} + c_Q = 0 \quad (3)$$

where the corresponding coefficients of the equation are expressed as below:

$$\begin{cases} a_Q = \dfrac{r_{\mathrm{r}} (x_{\mathrm{s}} + x_{\mathrm{m}})^2}{x_{\mathrm{m}}^2 V^2} \left(\dfrac{1}{\tan^2 \varphi_{\mathrm{s}}} + 1\right) \\ b_Q = \dfrac{1 - s}{\tan \varphi_{\mathrm{s}}} + \dfrac{2 r_{\mathrm{r}} (x_{\mathrm{s}} + x_{\mathrm{m}})}{x_{\mathrm{m}}^2} \\ c_Q = \dfrac{r_{\mathrm{r}} V^2}{x_{\mathrm{m}}^2} - \dfrac{P_{\mathrm{wf}}}{n_{\mathrm{wt}}} \end{cases} \quad (4)$$

where V is the bus voltage; r_{r}, x_{s}, and x_{m} are the rotor resistance, stator reactance, and magnetizing reactance of wind turbine respectively; φ_{s} is the stator side power factor angle; s is the slip and can be obtained according to the relationship

between slip and rotor speed, which is given as below:

$$s = \frac{n_{\text{syn}} - n}{n_{\text{syn}}} = \begin{cases} 1 - \dfrac{n_{\min}}{n_{\text{syn}}} & 0 < \dfrac{P_{\text{wf}}}{n_{\text{wt}}} \le P_1 \\ 1 - \dfrac{1}{n_{\text{syn}}} \sqrt[3]{\dfrac{P_{\text{wf}}/n_{\text{wt}}}{k_{\text{opt}}}} & P_1 < \dfrac{P_{\text{wf}}}{n_{\text{wt}}} \le P_2 \\ 0 & P_2 < \dfrac{P_{\text{wf}}}{n_{\text{wt}}} \le P_3 \\ \left(1 - \dfrac{n_{\max}}{n_{\text{syn}}}\right)^{\frac{P_{\text{wf}}/n_{\text{wt}} - P_3}{P_{\max} - P_3}} & P_3 < \dfrac{P_{\text{wf}}}{n_{\text{wt}}} \le P_{\max} \end{cases} \quad (5)$$

where n is the rotor speed; $n_{\min}$, n_{syn}, and $n_{\max}$ are the minimum, synchronous, and maximum speeds of rotor respectively; k_{opt} is the active power versus wind speed conversion parameter; P_1, P_2, and P_3 are the active power thresholds; $P_{\max}$ is the maximum active power.

For a PMSG-based wind farm, it is assumed to be operated in constant power factor control mode [16]. Therefore, the reactive power is the product of the active power and the tangent of power factor angle φ:

$$Q_{\text{wf}} = P_{\text{wf}} \tan \varphi \quad (6)$$

C. SOLUTION TO POWER FLOW WITH MULTIPLE WIND FARMS

In the aforementioned DFIG-based wind farm model, the reactive power is the function of the active power and the bus voltage magnitude. Therefore, these buses connected to DFIG-based wind farms are considered as PQ buses with variable reactive power. To solve power flow integrating multiple wind farms, the joint iteration method [17] is employed in this paper, and the power injections of wind farms are moved to the right side of power flow equations to keep the left side constant:

$$\begin{cases} \boldsymbol{P}_{\text{g}} - \boldsymbol{P}_{\text{d}} = \boldsymbol{e} \circ (\boldsymbol{Ge} - \boldsymbol{Bf}) + \boldsymbol{f} \circ (\boldsymbol{Gf} - \boldsymbol{Be}) - \boldsymbol{P}_{\text{wf}} \\ \boldsymbol{Q}_{\text{g}} - \boldsymbol{Q}_{\text{d}} = \boldsymbol{f} \circ (\boldsymbol{Ge} - \boldsymbol{Bf}) - \boldsymbol{e} \circ (\boldsymbol{Gf} - \boldsymbol{Be}) - \boldsymbol{Q}_{\text{wf}} \end{cases} \quad (7)$$

where $\boldsymbol{P}_{\text{g}}$, $\boldsymbol{P}_{\text{d}}$, and $\boldsymbol{P}_{\text{wf}}$ are the column vectors of active power of conventional generation units, loads, and wind farms respectively; $\boldsymbol{Q}_{\text{g}}$, $\boldsymbol{Q}_{\text{d}}$, and $\boldsymbol{Q}_{\text{wf}}$ are the column vectors of reactive power of conventional generation units, loads, and wind farms respectively; $\boldsymbol{e}$ and $\boldsymbol{f}$ are the column vectors of bus voltage rectangular components; $\boldsymbol{G}$ and $\boldsymbol{B}$ are the conductance and susceptance matrices respectively; $\circ$ denotes the Hadamard product of matrices. For each DFIG-based wind farm, the following terms are subtracted from their corresponding elements in the Jacobian matrix during the Newton-Raphson iteration process:

$$\begin{cases} \dfrac{\partial Q_{\text{wf},i}}{\partial e_i} = \dfrac{2e_i}{V_i^2} \left(Q_{\text{wf},i} - \dfrac{P_{\text{wf},i}}{\sqrt{\Delta_{Q,i}}} \right) \\ \dfrac{\partial Q_{\text{wf},i}}{\partial f_i} = \dfrac{2f_i}{V_i^2} \left(Q_{\text{wf},i} - \dfrac{P_{\text{wf},i}}{\sqrt{\Delta_{Q,i}}} \right) \end{cases} \quad (8)$$

where $\Delta_{Q,i}$ is the discriminant of the quadratic equation for DFIG-based wind farm at bus i, and $\Delta_{Q,i} = b2\ Q, i - 4a_{Q,i}c_{Q,i}$.

III. OPF WITH WIND GENERATION AND POWER GRID UNCERTAINTIES

A. THE MIXED ET AND AA UNCERTAINTY PROPAGATION FRAMEWORK

In ET, a Dempster-Shafer structure (DS) simultaneously represents aleatory and epistemic uncertainties of a variable, identified with its basic probability assignment m:

$$m : 2^{\Omega} \to [0, 1], \quad m(\emptyset) = 0, \quad \sum_{a \in 2^{\Omega}} m(a) = 1 \quad (9)$$

where Ω is the universe; 2^{Ω} is the power set of all subsets of Ω; the sets in 2^{Ω} with non-zero masses are called focal elements. Each DS corresponds to a plausibility measure Pl and a belief measure Bel:

$$\begin{cases} Bel(a) = \sum_{b \subseteq a} m(b) \\ Pl(a) = \sum_{b \cap a \neq \emptyset} m(b) \end{cases} \quad (10)$$

These measures bound the probability P of any set a in 2^{Ω}:

$$\text{Bel}(a) \le \text{P}(a) \le \text{Pl}(a) \quad (11)$$

Hence the cumulative plausibility and belief of a DS on the real line form a probability box (p-box), and conversely, a p-box corresponds to an equivalence class of DSs [18]. Namely, DSs and p-boxes are interconvertible. With possibility theory being a special branch of ET with nested focal elements, a possibility distribution can be interpreted as a family of probability distributions with the possibility and necessity measures as its bounds [19]. In this work, a DS of a real-valued variable X has a finite number n_X of closed intervals as focal elements and can be defined as a set of pairs of intervals x_i and masses $m_X(x_i)$, i.e., $\{(x_i, m_X(x_i)) | i = 1, \ldots, n_X\}$. Thus, probability distributions, possibility distributions, and intervals can be encoded into finite DSs [18], [20].

When a binary arithmetic operation $\square$ performs on two variables X and Y, convolution takes place between their DSs, $\{(x_i, m_X(x_i)) | i = 1, \ldots, n_X\}$ and $\{(y_j, m_Y(y_j)) | j = 1, \ldots, n_Y\}$, to produce the DS of the arithmetic result Z. For independent variables, the result is a Cartesian product of the operands, denoted by $\{(z_{ij}, m_Z(z_{ij})) | i = 1, \ldots, n_X, j = 1, \ldots, n_Y\}$, and the associated masses are the products of corresponding masses [21]:

$$Z = X \square Y : z_{ij} = x_i \square y_j, m_Z(z_{ij}) = m_X(x_i)\, m_Y(y_j) \quad (12)$$

For variables with dependence modeled by a copula C fitted to historical statistics, the result is also a Cartesian product, with the associated masses calculated using the copula [21]:

$$Z = X \square Y : z_{ij} = x_i \square y_j,$$

$$m_Z\left(z_{ij}\right) = C\left(X_i, Y_j\right) - C\left(X_{i-1}, Y_j\right) - C\left(X_i, Y_{j-1}\right) + C\left(X_{i-1}, Y_{j-1}\right) \quad (13)$$

where x_i and y_j are sorted or transformed without altering the cumulative plausibility and belief to satisfy $\inf(x_{i-1}) \leq \inf(x_i)$, $\sup(x_{i-1}) \leq \sup(x_i)$, $\inf(y_{j-1}) \leq \inf(y_j)$, and $\sup(y_{j-1}) \leq \sup(y_j)$; X_i and Y_j are the cumulative masses:

$$\begin{cases} X_i = \sum_{k=1}^{i} m_X\left(x_k\right) \\ Y_j = \sum_{k=1}^{j} m_Y\left(y_k\right) \end{cases} \quad (14)$$

For variables with extreme dependence, the conversions between DSs and p-boxes are utilized to calculate the convolution in the form of p-boxes. Regarding the p-boxes of X, Y, and Z denoted by $[\bar{F}_X, \underline{F}_X]$, $[\bar{F}_Y, \underline{F}_Y]$, and $[\bar{F}_Z, \underline{F}_Z]$ respectively, the convolutions under perfect and opposite dependence can be expressed in (15) and (16) respectively $(0 \leq p \leq 1)$ [21]:

$$\begin{cases} \bar{F}_Z^{-1}(p) = \inf\limits_{\substack{F_X \in [\bar{F}_X, \underline{F}_X] \\ F_Y \in [\bar{F}_Y, \underline{F}_Y]}} \left[F_X^{-1}(p) \square F_Y^{-1}(p)\right] \\ \underline{F}_Z^{-1}(p) = \sup\limits_{\substack{F_X \in [\bar{F}_X, \underline{F}_X] \\ F_Y \in [\bar{F}_Y, \underline{F}_Y]}} \left[F_X^{-1}(p) \square F_Y^{-1}(p)\right] \end{cases} \quad (15)$$

$$\begin{cases} \bar{F}_Z^{-1}(p) = \inf\limits_{\substack{F_X \in [\bar{F}_X, \underline{F}_X] \\ F_Y \in [\bar{F}_Y, \underline{F}_Y]}} \left[F_X^{-1}(p) \square F_Y^{-1}(1-p)\right] \\ \underline{F}_Z^{-1}(p) = \sup\limits_{\substack{F_X \in [\bar{F}_X, \underline{F}_X] \\ F_Y \in [\bar{F}_Y, \underline{F}_Y]}} \left[F_X^{-1}(p) \square F_Y^{-1}(1-p)\right] \end{cases} \quad (16)$$

For variables with unknown dependence, the pointwise tightest probability bounds guaranteed to enclose the actual probability distribution are calculated according to the Fréchet-Hoeffding limits [21], [22]:

$$\begin{cases} \bar{F}_Z(z) = \inf\limits_{\substack{z = x \square y \\ F_X \in [\bar{F}_X, \underline{F}_X] \\ F_Y \in [\bar{F}_Y, \underline{F}_Y]}} \min\left[F_X(x) + F_Y(y), 1\right] \\ \underline{F}_Z(z) = \sup\limits_{\substack{z = x \square y \\ F_X \in [\bar{F}_X, \underline{F}_X] \\ F_Y \in [\bar{F}_Y, \underline{F}_Y]}} \max\left[F_X(x) + F_Y(y) - 1, 0\right] \end{cases} \quad (17)$$

The number of focal elements is limited via approximations of DSs to avoid its exponential growth and keep the computation tractable [22].

Variables in a nonlinear system of equations have complex dependencies that cannot be determined easily. Uncertainty propagation with unjustified assumption of independence or total ignorance about dependence in the arithmetic process can result in probability bounds much narrower or wider than actual quantities [21]. Here, an extension of AA [23], is introduced to record the first and the second order correlations between variables and noise symbols, which are the normalized uncertain inputs of the system, and add structure to DS arithmetic. In this mixed framework, a quantity is represented by a quadratic form (QF) with DS noise symbols:

$$\hat{x} = x_0 + \boldsymbol{x}_1\boldsymbol{\varepsilon} + \boldsymbol{\varepsilon}^{\mathrm{T}}\boldsymbol{x}_2\boldsymbol{\varepsilon} \quad (18)$$

where x_0 is the central value; $\boldsymbol{x}_1$ and $\boldsymbol{x}_2$ are the matrices of partial deviations representing the first and the second order correlations with noise symbols respectively; $\boldsymbol{\varepsilon}$ is the column vector of DS noise symbols. The omission of error-related terms from conventional AA costs QF the self-validation feature but reduces computational burden significantly whilst still being adequately accurate in the practice of power flow calculation. Arithmetic operations on QFs are described as below:

$$\begin{cases} \alpha \pm \hat{x} = (\alpha \pm x_0) \pm \boldsymbol{x}_1\boldsymbol{\varepsilon} \pm \boldsymbol{\varepsilon}^{\mathrm{T}}\boldsymbol{x}_2\boldsymbol{\varepsilon} \\ \alpha \cdot \hat{x} = \alpha x_0 + (\alpha \boldsymbol{x}_1)\boldsymbol{\varepsilon} + \boldsymbol{\varepsilon}^{\mathrm{T}}(\alpha \boldsymbol{x}_2)\boldsymbol{\varepsilon} \\ \hat{x} \pm \hat{y} = (x_0 \pm y_0) + (\boldsymbol{x}_1 \pm \boldsymbol{y}_1)\boldsymbol{\varepsilon} + \boldsymbol{\varepsilon}^{\mathrm{T}}(\boldsymbol{x}_2 \pm \boldsymbol{y}_2)\boldsymbol{\varepsilon} \\ \hat{x} \cdot \hat{y} = x_0 y_0 + (y_0 \boldsymbol{x}_1 + x_0 \boldsymbol{y}_1)\boldsymbol{\varepsilon} \\ \qquad + \boldsymbol{\varepsilon}^{\mathrm{T}}(y_0 \boldsymbol{x}_2 + x_0 \boldsymbol{y}_2 + \boldsymbol{x}_1^{\mathrm{T}} \boldsymbol{y}_1)\boldsymbol{\varepsilon} \end{cases} \quad (19)$$

where α is a real number. A QF with DS noise symbols can be converted into a corresponding DS with the help of summing up the QF terms via convolution, which is called concretization [24] and denoted by DS $(\hat{x})$.

B. INCORPORATING WIND FARMS INTO UNCERTAIN POWER FLOW

A general framework of uncertain power flow based on ET and AA has been proposed in [25]. Based on the framework, an ad-hoc probabilistic model of wind farm active power [14], derived from the wind speed probability distribution (two-parameter Weibull distribution is used here) and the wind farm active power versus wind speed curve, is adopted to represent the uncertainty of wind generation, in the form of cumulative distribution function (CDF) as described below:

$$F\left(P_{\mathrm{wf}}\right) = \begin{cases} 0 & P_{\mathrm{wf}} < 0 \\ -\exp\left\{-\frac{1}{(\xi_{\mathrm{wf}}\lambda)^k} \cdot \left[\frac{P_{\mathrm{wf}}}{P_{\mathrm{wfr}}}\left(v_{\mathrm{r}}^3 - v_{\mathrm{ci}}^3\right) + v_{\mathrm{ci}}^3\right]^{k/3}\right\} & \\ \quad + \exp\left[-\left(\frac{v_{\mathrm{co}}}{\lambda}\right)^k\right] + 1 & 0 \leq P_{\mathrm{wf}} < P_{\mathrm{wfr}} \\ 1 & P_{\mathrm{wf}} \geq P_{\mathrm{wfr}} \end{cases} \quad (20)$$

where k and λ are the shape and scale parameters of Weibull distribution respectively. Calculating the DFIG-based wind farm reactive power involves the slip, of which the expression is a piecewise function across the range of active power output. Being non-affine, the slip function needs to be approximated as an affine operation on QFs, and the Remez algorithm is used to obtain the minimax approximation:

$$\hat{s} = s_{\mathrm{a}2}\hat{P}_{\mathrm{wf}}^2 + s_{\mathrm{a}1}\hat{P}_{\mathrm{wf}} + s_{\mathrm{a}0} + \hat{s}_{\mathrm{err}} \quad (21)$$

where s_{a2}, s_{a1}, and s_{a0} are the coefficients of the approximating polynomial; $\hat{s}_{err}$ is the approximation error, added to the expression to bound the actual slip and taken as an additional uncertain input:

$$\hat{s}_{err} = s_{err}^{max} \varepsilon_{err} \tag{22}$$

where s_{err}^{max} is the maximum approximation error; ε_{err} is an interval with a range of $[-1, 1]$.

Let the column vector $\boldsymbol{u}$ denote the uncertain inputs, namely wind farm active power and other variable parameters of the power grid, then the noise symbols can be obtained via normalization:

$$\boldsymbol{\varepsilon} = \Delta \boldsymbol{u}^{-1} \left(\boldsymbol{u} - \boldsymbol{u}^0 \right) \tag{23}$$

where $\boldsymbol{u}^0$ is the column vector of the range midpoints of the uncertain inputs, forming the central operating point; $\Delta \boldsymbol{u}$ is the diagonal matrix of the range radiuses of the uncertain inputs. Utilizing Taylor series expansion at the central operating point, the expressions of the QFs of bus voltage rectangular components are given below:

$$\begin{cases} \hat{e}_i = e_i^0 + \left(\dfrac{\partial e_i}{\partial \boldsymbol{u}^{\mathrm{T}}} \bigg|_0 \Delta \boldsymbol{u} \right) \boldsymbol{\varepsilon} + \boldsymbol{\varepsilon}^{\mathrm{T}} \left(\dfrac{1}{2} \Delta \boldsymbol{u} \dfrac{\partial^2 e_i}{\partial \boldsymbol{u}^2} \bigg|_0 \Delta \boldsymbol{u} \right) \boldsymbol{\varepsilon} \\ \hat{f}_i = f_i^0 + \left(\dfrac{\partial f_i}{\partial \boldsymbol{u}^{\mathrm{T}}} \bigg|_0 \Delta \boldsymbol{u} \right) \boldsymbol{\varepsilon} + \boldsymbol{\varepsilon}^{\mathrm{T}} \left(\frac{1}{2} \Delta \boldsymbol{u} \dfrac{\partial^2 f_i}{\partial \boldsymbol{u}^2} \bigg|_0 \Delta \boldsymbol{u} \right) \boldsymbol{\varepsilon} \end{cases} \tag{24}$$

The central values can be obtained by solving the power flow at the central operating point. Obviously, the partial derivatives for the slack bus are zero. For other buses, the partial derivatives are calculated by solving the following linear systems derived from the power flow equations. Now suppose that buses 1 to M, $M+1$ to $N-1$, and N are PQ buses, PV buses, and slack bus respectively, and u and w denote any of the uncertain inputs. For the first-order partial derivatives:

$$\boldsymbol{J} \cdot \begin{bmatrix} \dfrac{\partial \boldsymbol{e}'}{\partial u} \\ \dfrac{\partial \boldsymbol{f}'}{\partial u} \end{bmatrix} = \left[\eta_1^P, \ldots, \eta_{N-1}^P, \eta_1^Q, \ldots, \eta_M^Q, \eta_{M+1}^V, \ldots, \eta_{N-1}^V \right]^{\mathrm{T}} \tag{25}$$

where $\boldsymbol{J}$ is the Jacobian matrix; $\boldsymbol{e}'$ and $\boldsymbol{f}'$ are the column vectors of bus voltage rectangular components sans the slack bus; the constant terms of the linear system are expressed as below:

$$\begin{cases} \eta_i^P = \dfrac{\partial P_{g,i}}{\partial u} - \dfrac{\partial P_{d,i}}{\partial u} + \dfrac{\partial P_{wf,i}}{\partial u} \\ \eta_i^Q = \dfrac{\partial Q_{g,i}}{\partial u} - \dfrac{\partial Q_{d,i}}{\partial u} + \dfrac{\partial Q_{wf,i}}{\partial u} \\ \eta_i^V = \dfrac{\partial V_i}{\partial u} \end{cases} \tag{26}$$

and the partial derivative of wind farm reactive power depends on the type of wind farm connecting to bus i:

$$\frac{\partial Q_{wf,i}}{\partial u} = \begin{cases} \dfrac{1}{\sqrt{\Delta_{Q,i}}} \left(\dfrac{Q_{wf,i}}{\tan \varphi_{s,i}} \dfrac{\partial s_i}{\partial P_{wf,i}} + 1 \right) \dfrac{\partial P_{wf,i}}{\partial u} \\ \quad + \dfrac{Q_{wf,i}}{\sqrt{\Delta_{Q,i}} \tan \varphi_{s,i}} \dfrac{\partial s_{err,i}}{\partial u} & \text{DFIG} \\ \tan \varphi_i \dfrac{\partial P_{wf,i}}{\partial u} & \text{PMSG} \end{cases} \tag{27}$$

For the second-order partial derivatives:

$$\boldsymbol{J} \cdot \begin{bmatrix} \dfrac{\partial^2 \boldsymbol{e}'}{\partial u \partial w} \\ \dfrac{\partial^2 \boldsymbol{f}'}{\partial u \partial w} \end{bmatrix} = \Big[\mu_1^P, \ldots, \mu_{N-1}^P, \mu_1^Q, \ldots, \mu_M^Q, \mu_{M+1}^V, \ldots, \mu_{N-1}^V \Big]^{\mathrm{T}} \tag{28}$$

where the constant terms of the linear system are expressed as below:

$$\begin{cases} \mu_i^P = -\dfrac{\partial e_i}{\partial u} \dfrac{\partial I_{re,i}}{\partial w} - \dfrac{\partial e_i}{\partial w} \dfrac{\partial I_{re,i}}{\partial u} - \dfrac{\partial f_i}{\partial u} \dfrac{\partial I_{im,i}}{\partial w} - \dfrac{\partial f_i}{\partial w} \dfrac{\partial I_{im,i}}{\partial u} \\ \mu_i^Q = -\dfrac{\partial f_i}{\partial u} \dfrac{\partial I_{re,i}}{\partial w} - \dfrac{\partial f_i}{\partial w} \dfrac{\partial I_{re,i}}{\partial u} + \dfrac{\partial e_i}{\partial u} \dfrac{\partial I_{im,i}}{\partial w} + \dfrac{\partial e_i}{\partial w} \dfrac{\partial I_{im,i}}{\partial u} \\ \qquad + \mu_i^{Q,wf} \\ \mu_i^V = \dfrac{1}{V_i} \left(\dfrac{\partial V_i}{\partial u} \dfrac{\partial V_i}{\partial w} - \dfrac{\partial e_i}{\partial u} \dfrac{\partial e_i}{\partial w} - \dfrac{\partial f_i}{\partial u} \dfrac{\partial f_i}{\partial w} \right) \end{cases} \tag{29}$$

where $I_{re,i}$ and $I_{im,i}$ are the real and imaginary parts of nodal current injection at bus i respectively, and their partial derivatives are given below:

$$\begin{cases} \dfrac{\partial I_{re,i}}{\partial u} = \displaystyle\sum_{j=1}^{N-1} \left(G_{ij} \dfrac{\partial e_j}{\partial u} - B_{ij} \dfrac{\partial f_j}{\partial u} \right) \\ \dfrac{\partial I_{im,i}}{\partial u} = \displaystyle\sum_{j=1}^{N-1} \left(G_{ij} \dfrac{\partial e_j}{\partial u} + B_{ij} \dfrac{\partial f_j}{\partial u} \right) \end{cases} \tag{30}$$

The term $\mu_i^{Q,wf}$ has the following expression if a DFIG-based wind farm is connected to bus i, which otherwise equals zero:

$$\begin{aligned} \lambda_i^{Q,wf} = {} & \frac{2}{V_i^2} \left(Q_{wf,i} - \frac{P_{wf,i}}{\sqrt{\Delta_{Q,i}}} \right) \left(\frac{\partial e_i}{\partial u} \frac{\partial e_i}{\partial w} + \frac{\partial f_i}{\partial u} \frac{\partial f_i}{\partial w} \right) \\ & + \frac{Q_{wf,i}}{\sqrt{\Delta_{Q,i}} \tan \varphi_{s,i}} \left[\frac{\partial^2 s_i}{\partial P_{wf,i}^2} \frac{\partial P_{wf,i}}{\partial u} \frac{\partial P_{wf,i}}{\partial w} \right. \\ & \left. + \frac{1}{V_i^2} \left(\frac{\partial V_i^2}{\partial u} \frac{\partial s_i}{\partial w} + \frac{\partial V_i^2}{\partial w} \frac{\partial s_i}{\partial u} \right) \right] \\ & - \frac{2 a_{Q,i}}{n_{wt,i} \Delta_{Q,i}^{3/2}} \left(\frac{P_{wf,i}}{V_i^2} \frac{\partial V_i^2}{\partial u} - \frac{\partial P_{wf,i}}{\partial u} \right) \\ & \times \left(\frac{P_{wf,i}}{V_i^2} \frac{\partial V_i^2}{\partial w} - \frac{\partial P_{wf,i}}{\partial w} \right) \end{aligned}$$

$$-\frac{b_{Q,i}}{\Delta_{Q,i}^{3/2}\tan\varphi_{s,i}}\left[\left(\frac{P_{wf,i}}{V_i^2}\frac{\partial V_i^2}{\partial u}-\frac{\partial P_{wf,i}}{\partial u}\right)\frac{\partial s_i}{\partial w}+\left(\frac{P_{wf,i}}{V_i^2}\frac{\partial V_i^2}{\partial w}-\frac{\partial P_{wf,i}}{\partial w}\right)\frac{\partial s_i}{\partial u}\right]-\frac{2n_{wt,i}c_{Q,i}}{\Delta_{Q,i}^{3/2}\tan^2\varphi_{s,i}}\frac{\partial s_i}{\partial u}\frac{\partial s_i}{\partial w} \tag{31}$$

where

$$\begin{cases}\dfrac{\partial V_i^2}{\partial u}=2e_i\dfrac{\partial e_i}{\partial u}+2f_i\dfrac{\partial f_i}{\partial u}\\ \dfrac{\partial s_i}{\partial u}=\dfrac{\partial s_i}{\partial P_{wf,i}}\dfrac{\partial P_{wf,i}}{\partial u}+\dfrac{\partial s_{err,i}}{\partial u}\end{cases} \tag{32}$$

The uncertain power flow is then solved by calculating the QFs of variables using AA according to the power flow equations and converting them into DSs.

C. PROBLEM FORMULATION

Based on the aforementioned uncertain power flow method, an OPF model incorporating multiple wind farms and other uncertain factors (e.g. loads) in a power system is proposed in this paper. Here, the objective function is minimizing the active power loss P_{loss} of the power system:

$$\min DS\left(\hat{P}_{loss}\right)=\mathrm{DS}\left(\sum_i \hat{P}_{g,i}+\hat{P}_{wf,i}-\hat{P}_{d,i}\right) \tag{33}$$

The control variables include the active power outputs of conventional generation units $P_{g,i}$ at PV buses, and the voltage magnitudes V_i of PV buses and slack bus. The power flow equations, expressed in QFs, are the equality constraints:

$$\begin{cases}\hat{\boldsymbol{P}}_g-\hat{\boldsymbol{P}}_d=\hat{\boldsymbol{e}}\circ\left(\boldsymbol{G}\hat{\boldsymbol{e}}-\boldsymbol{B}\hat{\boldsymbol{f}}\right)+\hat{\boldsymbol{f}}\circ\left(\boldsymbol{G}\hat{\boldsymbol{f}}-\boldsymbol{B}\hat{\boldsymbol{e}}\right)-\hat{\boldsymbol{P}}_{wf}\\ \hat{\boldsymbol{Q}}_g-\hat{\boldsymbol{Q}}_d=\hat{\boldsymbol{f}}\circ\left(\boldsymbol{G}\hat{\boldsymbol{e}}-\boldsymbol{B}\hat{\boldsymbol{f}}\right)-\hat{\boldsymbol{e}}\circ\left(\boldsymbol{G}\hat{\boldsymbol{f}}-\boldsymbol{B}\hat{\boldsymbol{e}}\right)-\hat{\boldsymbol{Q}}_{wf}\end{cases} \tag{34}$$

The inequality constraints include: lower and upper limits on the active and reactive power outputs of conventional generation units, $P_{g,i}^{min}$, $P_{g,i}^{max}$, $Q_{g,i}^{min}$, and $Q_{g,i}^{max}$; lower and upper limits on the bus voltage magnitudes, V_i^{min} and V_i^{max}; upper limits on the apparent power of branches, S_{ij}^{max}. The control variables in these constraints are expressed in real numbers:

$$\begin{cases}P_{g,i}^{min}\le P_{g,i}\le P_{g,i}^{max}\\ V_i^{min}\le V_i\le V_i^{max}\end{cases} \tag{35}$$

The state variables in these constraints are expressed in DSs:

$$\begin{cases}P_{g,i}^{min}\le DS\left(\hat{P}_{g,i}\right)\le P_{g,i}^{max}\\ Q_{g,i}^{min}\le DS\left(\hat{Q}_{g,i}\right)\le Q_{g,i}^{max}\\ V_i^{min}\le\sqrt{DS\left(\hat{e}_i^2+\hat{f}_i^2\right)}\le V_i^{max}\\ \sqrt{DS\left(\hat{P}_{ij}\right)^2+DS\left(\hat{Q}_{ij}\right)^2}\le S_{ij}^{max}\end{cases} \tag{36}$$

IV. SOLUTION METHODOLOGY

A. PSO

The existing OPF algorithms are incapable to handle uncertain variables described by DSs. The PSO, with its advantages being easy implementation, low number of parameters, and relative computational efficiency, is therefore combined with the following techniques of fitness comparison and constraint handling for DSs to solve the proposed uncertain OPF model. The local best model with the von Neumann neighborhood topology is employed, and the PSO algorithm is further enhanced by a stability-based adaptive inertia weight strategy [26], where the social and cognitive scaling parameters are also adjusted accordingly. The initial velocities are set to be zero to reduce roaming particles [27], and infeasible particles are brought back into the feasible region by mirroring the positions and setting the velocities to be zero in the violated dimensions [28].

B. FITNESS COMPARISON

A ranking method in ET based on the probability bounds of the difference for fitness comparison has been proposed in [29]. However, in practice a good number of solutions will be classified as equivalent ones when there are large overlaps among the fitness DSs. In this work, a quantile-based method of comparing DS fitness for optimization problem is proposed.

We first take a look at the probabilistic fitness. Suppose that X and Y are the fitness to be compared, and their quantile functions are Q_X and Q_Y respectively. For a minimization problem, X is deemed better than Y if the following statement is true:

$$\left(\forall p\in[0,1],Q_X(p)\le Q_Y(p)\right)\wedge\left(\exists p_0\in[0,1],Q_X(p_0)\ne Q_Y(p_0)\right) \tag{37}$$

Please note that X and Y are deemed equal only if their quantile functions are exactly the same. If Q_X is less than Q_Y at some probability levels and greater than Q_Y at others, X and Y are considered as "no better no worse" rather than equal.

A DS fitness is converted into a p-box and interpreted as the bounds on the quantile at any probability level. As a p-box represents a class of probability distributions, the bounds are essentially quantile functions and can be compared using the aforementioned method. The principle of comparison is to get the fitness minimized in its entirety. That is, the better fitness has either 1) a better left bound and a better or equal right bound, or 2) an equal left bound and a better right bound. Therefore, the comparison is purely based on the relations between the bounds of p-boxes and not hindered by overlapping.

C. CONSTRAINT HANDLING

In the constraints, a DS is also converted into a p-box but interpreted differently as the bounds on the cumulative probability associated with any quantity value. Then the lower and

upper probabilities of a variable X satisfying an inequality constraint can be obtained:

$$\begin{cases} \underline{F}_X(x) \le \mathrm{P}(X \le x) \le \bar{F}_X(x) \\ 1 - \bar{F}_X(x) \le \mathrm{P}(X \ge x) \le 1 - \underline{F}_X(x) \end{cases} \tag{38}$$

where $\bar{F}_X$ and $\underline{F}_X$ are the CDFs of the left and right bounds of X respectively. Thus an inequality constraint is taken as a chance constraint: it is considered satisfied as long as the lower probability is no less than its predetermined threshold. For violated constraints, the absolute differences between lower probabilities and thresholds are summed up as the constraint violation. In this way, the constraints and the objectives are handled separately. When comparing two solutions, the one with a smaller constraint violation is always preferred. If the solutions have equal constraint violations, the one with a better objective function value is preferred.

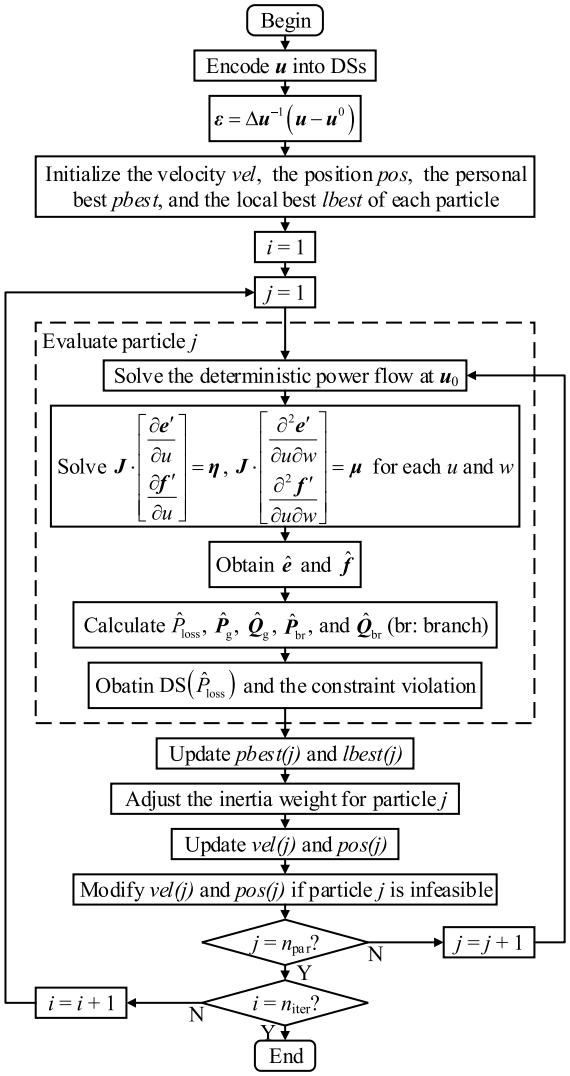

FIGURE 1. Flowchart of the enhanced PSO.

The flowchart of the enhanced PSO (EPSO) is shown in Fig. 1.

V. CASE STUDY

The proposed uncertain OPF model and the corresponding solution method are tested on the IEEE 30-bus standard test system and a real-sized 183-bus power system. All wind farms consist of either 1.5 MW DFIGs or 2MW PMSGs. The parameters of wind turbines can be referred to [16]. For the case studies, the parameters of Weibull distribution for wind speed probability distribution are assumed to be $k = 2.49$ and $\lambda = 6.85$ m/s. DSs in the uncertain power flow consists of 100 equiprobable focal elements. The thresholds for constraints on $P_{\mathrm{g},i}$, $Q_{\mathrm{g},i}$, V_i, and S_{ij} are set to be 1, 1, 0.9, and 0.9 respectively. All calculations are performed in the MATLAB$^{\mathrm{TM}}$ environment on a PC equipped with Intel Core i7-3770 3.4 GHz CPU and 8 GB RAM.

A. IEEE 30-BUS STANDARD TEST SYSTEM

Two wind farms are connected to the IEEE 30-bus standard test system at bus 6 and bus 28. The uncertain inputs of the test system and their dependencies are given in Table 1:

TABLE 1. Uncertain inputs in IEEE 30-bus standard test system.

Uncertain input	Mathematical model	Dependency
$P_{\mathrm{wf},6}$	Probability distribution	Gumbel copula [30], Kendall $\tau = 0.8$
$P_{\mathrm{wf},28}$	Probability distribution	
$P_{\mathrm{d},2}$	Triangular fuzzy number	Perfect dependence
$P_{\mathrm{d},12}$	Triangular fuzzy number	
$Q_{\mathrm{d},7}$	Interval	/
$Q_{\mathrm{d},24}$	Interval	/

* Uncertain inputs with unspecified dependency are independent.

The uncertain loads are modeled by triangular fuzzy numbers and intervals, varying around the center value with a certain load deviation. In this benchmark, the numbers of particles and iterations for EPSO are set to be 25 and 50 respectively.

In the first scenario, the optimal active power losses under different wind penetration levels are compared. The configurations of wind farms are shown in Table 2:

TABLE 2. Wind farms in IEEE 30-bus standard test system under different wind penetration levels.

Bus	Type	Wind penetration	n_{wt}	ξ_{wf}	P_{wfr}
6	DFIG	10%	16	0.9753	24 MW
		20%	32	0.9753	48 MW
		30%	56	0.9753	84 MW
28	PMSG	10%	12	0.9834	24 MW
		20%	24	0.9834	48 MW
		30%	42	0.9834	84 MW

The active and reactive loads at each bus increase at the same rate as the total generation capacity. With a 15% load deviation, the expressions of uncertain loads are listed in Table 3:

The optimal active power losses under 10%, 20%, and 30% wind penetration are presented as p-boxes shown in Fig. 2. As the wind penetration level increases, the p-box stretches towards higher active power loss. Even in the best case scenario where the actual probability distribution of active power

TABLE 3. Uncertain loads in IEEE 30-bus standard test system under different wind penetration levels.

Load	Wind penetration	Expression
$P_{d,2}$	10%	(18.59, 21.87, 25.15) MW
	20%	(20.58, 24.21, 27.85) MW
	30%	(23.57, 27.73, 31.89) MW
$P_{d,12}$	10%	(9.60, 11.29, 12.98) MW
	20%	(10.62, 12.50, 14.37) MW
	30%	(12.17, 14.32, 16.46) MW
$Q_{d,7}$	10%	[9.34, 12.63] Mvar
	20%	[10.34, 13.99] Mvar
	30%	[11.84, 16.02] Mvar
$Q_{d,24}$	10%	[5.74, 7.77] Mvar
	20%	[6.36, 8.60] Mvar
	30%	[7.28, 9.85] Mvar

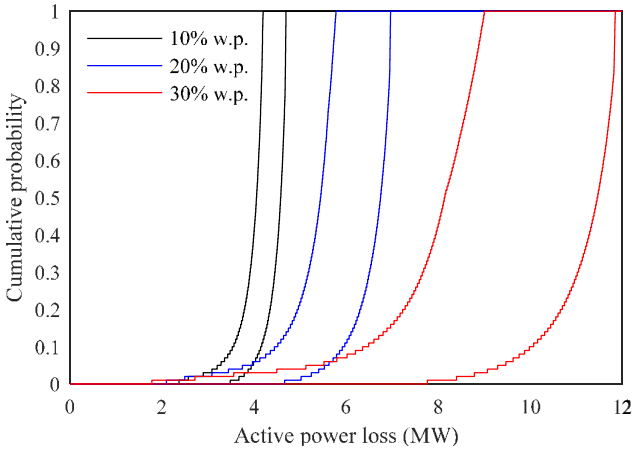

FIGURE 2. P-boxes of optimal active power losses of IEEE 30-bus standard test system under different wind penetration levels.

loss coincides with the left bound of p-box, the growth in wind generation makes the potential active power loss higher, more volatile, and thus more difficult to be managed.

In the second scenario, the optimal active power losses under different load deviation levels are compared. With a 20% wind penetration level, the expressions of uncertain loads are listed in Table 4:

TABLE 4. Uncertain loads in IEEE 30-bus standard test system under different load deviation levels.

Load	Load deviation	Expression
$P_{d,2}$	10%	(21.79, 24.21, 26.64) MW
	15%	(20.58, 24.21, 27.85) MW
	20%	(19.37, 24.21, 29.06) MW
$P_{d,12}$	10%	(11.25, 12.50, 13.75) MW
	15%	(10.62, 12.50, 14.37) MW
	20%	(10.00, 12.50, 15.00) MW
$Q_{d,7}$	10%	[10.95, 13.38] Mvar
	15%	[10.34, 13.99] Mvar
	20%	[9.73, 14.60] Mvar
$Q_{d,24}$	10%	[6.73, 8.22] Mvar
	15%	[6.36, 8.60] Mvar
	20%	[5.98, 8.97] Mvar

The optimal active power losses under 10%, 15%, and 20% load deviation are presented as p-boxes shown in Fig. 3.

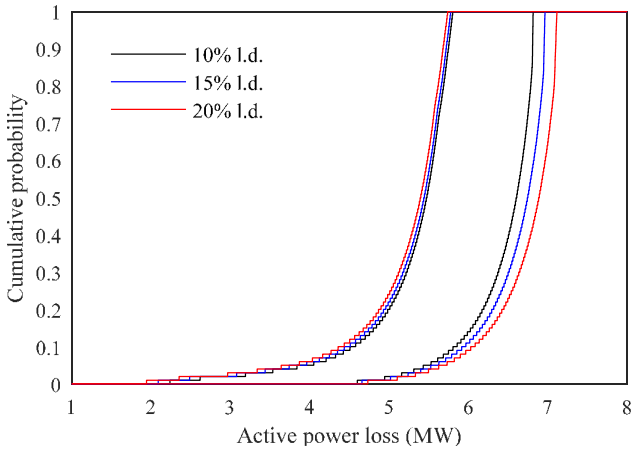

FIGURE 3. P-boxes of optimal active power losses of IEEE 30-bus standard test system under different load deviation levels.

TABLE 5. Uncertain inputs in real-sized 183-bus power system.

Uncertain input	Mathematical model	Dependency
$P_{wf,69}$	Probability distribution	Gumbel copula, Kendall $\tau = 0.6$
$P_{wf,156}$	Probability distribution	
$P_{d,72}$	Triangular fuzzy number	Perfect dependence
$P_{d,161}$	Triangular fuzzy number	
$Q_{d,149}$	Interval	/
$Q_{d,151}$	Interval	/

* Uncertain inputs with unspecified dependency are independent.

TABLE 6. Wind farms in real-sized 183-bus power system under different wind penetration levels.

Bus	Type	Wind penetration	n_{wt}	ξ_{wf}	P_{wfr}
69	DFIG	10%	360	0.9295	540 MW
		20%	810	0.8753	1215 MW
		30%	1392	0.8117	2088 MW
156	PMSG	10%	270	0.9295	540 MW
		20%	608	0.8690	1216 MW
		30%	1044	0.8117	2088 MW

The increase of load deviation has a different effect on the p-box: it gets wider, with the bounds seemingly moving towards both directions and keeping the shape. Therefore, a p-box of optimal active power loss is enclosed by another one under higher load deviation. This is due to the application of fuzzy numbers and intervals to modeling of uncertain loads, both of which bring epistemic uncertainty. As the potential active power loss is raised by a high load deviation, it is always desirable to reduce such uncertainty, by means of improving the accuracy of load forecast.

B. REAL-SIZED 183-BUS POWER SYSTEM

The real-sized power system consists of 183 buses, 308 branches, and 30 conventional generation units. The total generation capacity of conventional units is 9735 MW, and the active and reactive loads of the entire system are 6903.17 MW and 2637.17 Mvar respectively. Two wind farms are added at bus 69 and bus 156. The uncertain inputs of the system and their dependencies are given in Table 5:

TABLE 7. Uncertain loads in real-sized 183-bus power system under different wind penetration levels.

Load	Wind penetration	Expression
$P_{d,72}$	10%	(216.84, 255.11, 293.37) MW
	20%	(243.91, 286.95, 330.00) MW
	30%	(278.90, 328.12, 377.34) MW
$P_{d,161}$	10%	(488.41, 574.60, 660.79) MW
	20%	(549.39, 646.34, 743.29) MW
	30%	(628.21, 739.07, 849.93) MW
$Q_{d,149}$	10%	[110.20, 149.10] Mvar
	20%	[123.96, 167.71] Mvar
	30%	[141.75, 191.78] Mvar
$Q_{d,151}$	10%	[160.74, 217.47] Mvar
	20%	[180.80, 244.62] Mvar
	30%	[170.17, 255.25] Mvar

TABLE 8. Uncertain loads in real-sized 183-bus power system under different load deviation levels.

Load	Load deviation	Expression
$P_{d,72}$	10%	(258.26, 286.95, 315.65) MW
	15%	(243.91, 286.95, 330.00) MW
	20%	(229.56, 286.95, 344.34) MW
$P_{d,161}$	10%	(518.70, 646.34, 710.97) MW
	15%	(549.39, 646.34, 743.29) MW
	20%	(517.07, 646.34, 775.61) MW
$Q_{d,149}$	10%	[131.25, 160.42] Mvar
	15%	[123.96, 167.71] Mvar
	20%	[116.67, 175.01] Mvar
$Q_{d,151}$	10%	[191.44, 233.98] Mvar
	15%	[180.80, 244.62] Mvar
	20%	[170.17, 255.25] Mvar

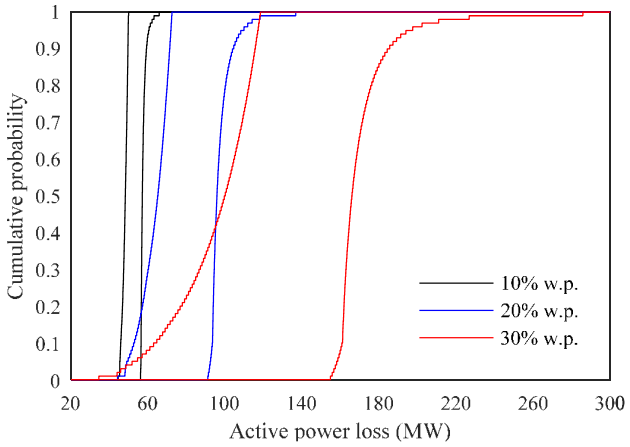

FIGURE 4. P-boxes of optimal active power losses of real-sized 183-bus power system under different wind penetration levels.

In this benchmark, the numbers of particles and iteration for PSO are set to be 64 and 100 respectively.

The same scenarios as in the previous case are studied. The configurations of wind farms under different wind penetration levels are shown in Table 6:

For the first scenario, the expressions of uncertain loads with a 15% load deviation are listed in Table 7:

For the second scenario, the expressions of uncertain loads with a 20% wind penetration level are listed in Table 8:

The optimal active power losses under different wind penetration levels and load deviation levels are presented as

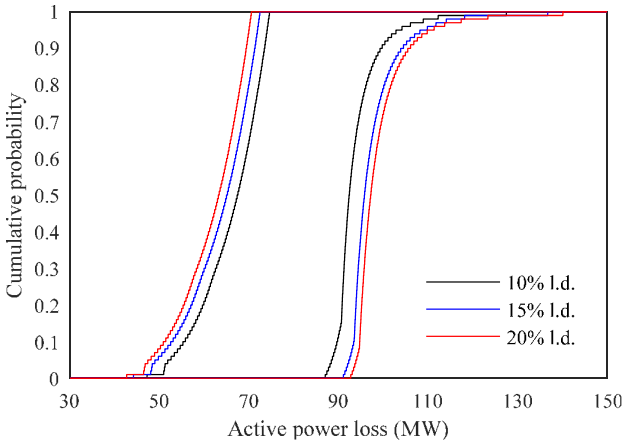

FIGURE 5. P-boxes of optimal active power losses of real-sized 183-bus power system under different load deviation levels.

p-boxes shown in Fig. 4 and Fig. 5 respectively. The results match the findings from the previous case, but the p-boxes obviously differ in shape. In the IEEE 30-bus standard test system, the probability masses of both the left and right bounds of optimal active power loss p-box lean to the right tail. Meanwhile, in the real-sized 183-bus power system, the probability masses are heavier on the right side with the left bound and on the left with the right bound.

VI. CONLUSION

A novel optimal power flow model incorporating wind generation and power grid uncertainties based on ET and AA is proposed in this paper. The properties of the active and reactive powers of wind farm are modeled and integrated into the power flow. With correlations and dependence handled in the DS arithmetic, the fusion of probabilistic, possibilistic, and interval uncertainties makes the most out of the available statistics to produce an accurate approximation of aleatory and epistemic uncertainties in the form of p-boxes at the optimal operating point, for a better understanding of the effect of uncertain factors on power systems. The validity of the proposed OPF model and solution are verified on the IEEE 30-bus test system and a real-sized 183-bus power system. It has to be pointed out that while the cases studied have only two wind farms and a low amount of uncertain parameters, the proposed approach can be generalized to more wind farms and more uncertain loads with high-dimensional dependencies and remain tractable by applying cost-saving techniques described in [1]. This proposed framework has the potential for broader applications in future power systems with high renewable penetration.

REFERENCES

[1] H. Zhang and P. Li, "Probabilistic analysis for optimal power flow under uncertainty," *IET Generat. Transmiss. Distrib.*, vol. 4, no. 5, pp. 553–561, May 2010.

[2] B. Zou and Q. Xiao, "Solving probabilistic optimal power flow problem using quasi Monte Carlo method and ninth-order polynomial normal transformation," *IEEE Trans. Power Syst.*, vol. 29, no. 1, pp. 300–306, Jan. 2014.

[3] M. Madrigal, K. Ponnambalam, and V. H. Quintana, "Probabilistic optimal power flow," in *Proc. IEEE Can. Conf. Elect. Comput. Eng.*, vol. 1. May 1998, pp. 385–388.
[4] A. Tamtum, A. Schellenberg, and W. D. Rosehart, "Enhancements to the cumulant method for probabilistic optimal power flow studies," *IEEE Trans. Power Syst.*, vol. 24, no. 4, pp. 1739–1746, Nov. 2009.
[5] D. Ke, C. Y. Chung, and Y. Sun, "A novel probabilistic optimal power flow model with uncertain wind power generation described by customized Gaussian mixture model," *IEEE Trans. Sustain. Energy*, vol. 7, no. 1, pp. 200–212, Jan. 2016.
[6] G. Verbic and C. A. Canizares, "Probabilistic optimal power flow in electricity markets based on a two-point estimate method," *IEEE Trans. Power Syst.*, vol. 21, no. 4, pp. 1883–1893, Nov. 2006.
[7] M. Aien, M. Rashidinejad, and M. F. Firuz-Abad, "Probabilistic optimal power flow in correlated hybrid wind-PV power systems: A review and a new approach," *Renew. Sustain. Energy Rev.*, vol. 41, pp. 1437–1446, Jan. 2015.
[8] V. Miranda and J. T. Saraiva, "Fuzzy modelling of power system optimal load flow," in *Proc. Power Ind. Comput. Appl. Conf.*, Baltimore, MD, USA, May 1991, pp. 386–392.
[9] X. Guan, W. H. E. Liu, and A. D. Papalexopoulos, "Application of a fuzzy set method in an optimal power flow," *Elect. Power Syst. Res.*, vol. 34, no. 1, pp. 11–18, Jul. 1995.
[10] R.-H. Liang, S.-R. Tsai, Y.-T. Chen, and W.-T. Tseng, "Optimal power flow by a fuzzy based hybrid particle swarm optimization approach," *Elect. Power Syst. Res.*, vol. 81, no. 7, pp. 1466–1474, Jul. 2011.
[11] A. Mohapatra, P. R. Bijwe, and B. K. Panigrahi, "Optimal power flow with multiple data uncertainties," *Elect. Power Syst. Res.*, vol. 95, pp. 160–167, Feb. 2013.
[12] M. Pirnia, C. A. Cañizares, K. Bhattacharya, and A. Vaccaro, "A novel affine arithmetic method to solve optimal power flow problems with uncertainties," *IEEE Trans. Power Syst.*, vol. 29, no. 6, pp. 2775–2783, Nov. 2014.
[13] A. Vaccaro and C. A. Cañizares, "An affine arithmetic-based framework for uncertain power flow and optimal power flow studies," *IEEE Trans. Power Syst.*, vol. 32, no. 1, pp. 274–288, Jan. 2017.
[14] L. B. Shi, Z. X. Weng, L. Z. Yao, and Y. X. Ni, "An analytical solution for wind farm power output," *IEEE Trans. Power Syst.*, vol. 29, no. 6, pp. 3122–3123, Nov. 2014.
[15] Z. X. Weng, L. B. Shi, Z. Xu, L. Z. Yao, Y. X. Ni, and M. Bazargan, "Effects of wind power variability and intermittency on power flow," in *Proc. IEEE Power Energy Soc. General Meeting*, San Diego, CA, USA, Jun. 2012, pp. 1–7.
[16] Z. Weng, L. Shi, Z. Xu, Q. Lu, L. Yao, and Y. Ni, "Fuzzy power flow solution considering wind power variability and uncertainty," *Int. Trans. Elect. Energy Syst.*, vol. 25, no. 3, pp. 547–572, Mar. 2015.
[17] H.-C. Wang, S.-X. Zhou, Z.-X. Lu, and J.-L. Wu, "A joint iteration method for load flow calculation of power system containing unified wind farm and its application," *Power Syst. Technol.*, vol. 29, no. 18, pp. 59–62, Sep. 2005.
[18] S. Ferson, V. Kreinovich, L. Ginzburg, D. S. Myers, and K. Sentz, "Constructing probability boxes and Dempster–Shafer structures," Sandia Nat. Labs., Albuquerque, NM, USA, Sandia Rep. SAND2002-4015, 2003.
[19] E. Zio and N. Pedroni, "Literature review of methods for representing uncertainty," FonCSI, Toulouse, France, Tech. Rep. 2013-03, 2013.
[20] C. Baudrit, D. Dubois, and D. Guyonnet, "Joint propagation and exploitation of probabilistic and possibilistic information in risk assessment," *IEEE Trans. Fuzzy Syst.*, vol. 14, no. 5, pp. 593–608, Oct. 2006.
[21] S. Ferson *et al.*, "Dependence in probabilistic modeling, Dempster-Shafer theory, and probability bounds analysis," Sandia Nat. Labs., Albuquerque, NM, USA, Sandia Rep. SAND2004-3072, 2004.
[22] R. C. Williamson and T. Downs, "Probabilistic arithmetic. I. Numerical methods for calculating convolutions and dependency bounds," *Int. J. Approx. Reasoning*, vol. 4, no. 2, pp. 89–158, Mar. 1990.
[23] F. Messine and A. Touhami, "A general reliable quadratic form: An extension of affine arithmetic," *Rel. Comput.*, vol. 12, no. 3, pp. 171–192, Jun. 2006.
[24] O. Bouissou, E. Goubault, J. Goubault-Larrecq, and S. Putot, "A generalization of p-boxes to affine arithmetic," *Springer Comput.*, vol. 94, no. 2, pp. 189–201, Mar. 2012.
[25] J. Luo, L. Shi, and Y. Ni, "Uncertain power flow analysis based on evidence theory and affine arithmetic," *IEEE Trans. Power Syst.*, vol. 33, no. 1, pp. 1113–1115, Jan. 2018.
[26] M. Taherkhani and R. Safabakhsh, "A novel stability-based adaptive inertia weight for particle swarm optimization," *Appl. Soft. Comput.*, vol. 38, pp. 281–295, Jan. 2016.
[27] A. Engelbrecht, "Particle swarm optimization: Velocity initialization," in *Proc. IEEE Congr. Evol. Comput.*, Brisbane, QLD, Australia, Jun. 2012, pp. 1–8.
[28] S. Helwig, J. Branke, and S. Mostaghim, "Experimental analysis of bound handling techniques in particle swarm optimization," *IEEE Trans. Evol. Comput.*, vol. 17, no. 2, pp. 259–271, Apr. 2013.
[29] M. Compare and E. Zio, "Genetic algorithms in the framework of Dempster-Shafer theory of evidence for maintenance optimization problems," *IEEE Trans. Rel.*, vol. 64, no. 2, pp. 645–660, Jun. 2015.
[30] P. Embrechts, F. Lindskog, and A. McNeil, "Modelling dependence with copulas and applications to risk management," in *Handbook of Heavy Tailed Distributions in Finance*. Amsterdam, The Netherlands: Elsevier, 2003, ch. 8, pp. 329–384.
[31] Y. Wang, N. Zhang, C. Kang, M. Miao, R. Shi, and Q. Xia, "An efficient approach to power system uncertainty analysis with high-dimensional dependencies," *IEEE Trans. Power Syst.*, to be published, doi: 10.1109/TPWRS.2017.2755698.

JINQING LUO received the B.S. degree in electrical engineering from Tsinghua University, Beijing, China, in 2015, where he is currently pursuing the M.Sc. degree with the National Key Laboratory of Power Systems in Shenzhen, Graduate School at Shenzhen.

His main research interest includes the uncertainty analysis of power system incorporating wind power.

Mr. Luo's awards and honors include the National Scholarship.

LIBAO SHI (M'04–SM'09) received the B.S., M.Sc., and Ph.D. degrees from the Department of Electrical Engineering, Chongqing University, Chongqing, China, in 1994, 1997, and 2000, respectively.

He was a Post-Doctoral Research Associate with the University of Hong Kong, China, from 2004 to 2006. He is currently an Associate Professor with the National Key Laboratory of Power Systems in Shenzhen, Graduate School at Shenzhen, Tsinghua University, Shenzhen, China. His research interests include complementary and coordinated dispatch and control with multi-energy source structure, power system cascading failure/restoration control, and power system stability analysis.

He is a member of the IET.

YIXIN NI (SM'94) received the B.S., M.Sc., and Ph.D. degrees in electrical engineering from Tsinghua University, Beijing, China.

She was an Associate Professor with the University of Hong Kong, China, from 1996 to 2007. She was also a former Professor and a Director of National Power System Laboratory, Tsinghua University, Beijing, China. She is currently the Professor of the National Key Laboratory of Power Systems in Shenzhen, Graduate School at Shenzhen, Tsinghua University, Shenzhen, China. Her research interests include power system stability and control, HVDC transmission, FACTS, and power markets.

Prof. Ni was a recipient of the National Excellent Science and Technology Books Award, Advanced Science and Technology Award of State Education Commission, and Government Special Financial Support.